Metal–Organic Frameworks

Nanospace Engineering of Metal–Organic Frameworks through Dynamic Spacer Installation of Multifunctionalities for Efficient Separation of Ethane from Ethane/Ethylene Mixtures

Cheng-Xia Chen, Zhang-Wen Wei, Tony Pham, Pui Ching Lan, Lei Zhang,
Katherine A. Forrest, Sha Chen, Abdullah M. Al-Enizi, Ayman Nafady, Cheng-Yong Su,* and
Shengqian Ma*

Abstract: *Herein, a dynamic spacer installation (DSI) strategy has been implemented to construct a series of multifunctional metal—organic frameworks (MOFs), LIFM-61/31/62/63, with optimized pore space and pore environment for ethane/ ethylene separation. In this respect, a series of linear dicarboxylic acids were deliberately installed in the prototype MOF, LIFM-28, leading to a dramatically increased pore volume (from 0.41 to 0.82 $cm^3 g^{-1}$) and reduced pore size (from 11.1 × 11.1 $Å^2$ to 5.6 × 5.6 $Å^2$). The increased pore volume endows the multifunctional MOFs with much higher ethane adsorption capacity, especially for LIFM-63 (4.8 $mmol\, g^{-1}$), representing nearly three times as much ethane as the prototypical counterpart (1.7 $mmol\, g^{-1}$) at 273 K and 1 bar. Meanwhile, the reduced pore size imparts enhanced ethane/ethylene selectivity of the multifunctional MOFs. Theoretical calculations and dynamic breakthrough experiments confirm that the DSI is a promising approach for the rational design of multifunctional MOFs for this challenging task.*

Introduction

As one of seven crucial chemical separations, olefin/ paraffin separation, accounting for about 0.3 % of global energy consumption, is of great significance in manufacturing industry.[1] As one of the most important olefins, ethylene (C_2H_4) is the largest raw material in petrochemical industries, with a global annual production of more than 170 million tons, corresponding to 26 kilograms for each person on the earth.[1] In general, it is produced via steam cracking or thermal decomposition of ethane (C_2H_6), followed by the distillation

purification from C_2H_6, in which a small amount of C_2H_6 impurity mixes into the product.[2] Thus, C_2H_6 needs to be removed from C_2H_4/C_2H_6 mixtures to produce poly-grade C_2H_4 feedstock for manufacturing plastics.[3] At present, the industrial separation of C_2H_4 from C_2H_6 is typically realized by cryogenic distillation at high pressure (5–28 bar) and low temperature (180–258 K),[1,4] leading to intensive energy consumption owing to their similar volatilities and sizes. Therefore, more cost- and energy-efficient separation technologies are highly desirable in the petrochemical industry. Among the new technologies, the adsorptive separation process based on porous solid materials has been considered as the most promising methodology.[5] Conventional solid adsorptive materials, such as zeolites,[5c,6] alumina,[7] and carbon-based materials,[8] have been explored for the C_2H_4/C_2H_6 separation but still can't fulfill the separation requirements of industrial demand due to their low adsorption capacity and separation selectivity. Owing to their structural diversity, tunable functionalities, designable pore sizes, and high pore volumes, metal-organic frameworks (MOFs) are expected to be the ideal candidate for the C_2H_4/C_2H_6 separation.[5b, 9]

The typical design strategies for the separation of C_2H_4/ C_2H_6 on MOFs mainly relies on the introduction of open metal sites (OMSs)[10] and Ag^I/Cu^I metal ions,[11] in which C_2H_4 can be preferentially captured as a result of the stronger affinities of the immobilized metal sites on the pore surfaces towards unsaturated C=C bond. Although these strategies have presented excellent adsorption separation performance for C_2H_4/C_2H_6 mixtures, the notorious problem with these

[*] Dr. C.-X. Chen, Dr. Z.-W. Wei, Prof. C.-Y. Su
MOE Laboratory of Bioinorganic and Synthetic Chemistry, Lehn Institute of Functional Materials, School of Chemistry, Sun Yat-Sen University, Guangzhou 510275 (China)
E-mail: cesscy@mail.sysu.edu.cn

Dr. C.-X. Chen, P. C. Lan, Prof. S. Ma
Department of Chemistry, University of North Texas CHEM 305D
1508 W Mulberry St, Denton, TX 76201 (USA)
E-mail: shengqian.ma@unt.edu

Dr. T. Pham, Dr. K. A. Forrest
Department of Chemistry, University of South Florida
4202 E. Fowler Avenue, Tampa, FL 33620 (USA)

Dr. L. Zhang
College of Materials Science and Engineering, Fujian University of Technology, Fuzhou 350118 (China)

Dr. S. Chen
Hunan Province Key Laboratory and Interface Science and Technology, School of Materials Science and Engineering, Central South University of Forestry and Technology
Changsha 410004 (China)

Prof. A. M. Al-Enizi, Prof. A. Nafady
Department of Chemistry, College of Science, King Saud University
Riyadh 11451 (Saudi Arabia)

Supporting information and the ORCID identification number(s) for the author(s) of this article can be found under:
https://doi.org/10.1002/anie.202100114.

approaches is that it is still energetically costly to produce poly-grade C_2H_4 raw materials during the desorption process owing to the formation of weak chemical bonds.[10c,11a] Furthermore, the MOFs constructed via these strategies usually suffer from stability and activity because of moisture sensitivity.[12] Therefore, it is imperative to develop C_2H_6-selective MOFs that can preferentially capture C_2H_6 over C_2H_4 by virtue of higher polarizability and more C−H bonds of C_2H_6. Compared to C_2H_4-selective MOFs, this approach seems to be more economical for C_2H_4/C_2H_6 separation, offering ~ 40 % of energy savings.[13] However, the MOFs with preferred C_2H_6 adsorption over C_2H_4 are scarce[9a,b,d–h,14] due to the difficulty to discriminate C_2H_6 over C_2H_4 or low C_2H_6 uptake resulting from small pore volume.

The key point to design C_2H_6-selective adsorbents is to achieve the combination of good selectivity and high uptake capacity, which however remains a daunting challenge. In this respect, Chen and Fedin groups have made some pioneering contributions in addressing the C_2H_4/C_2H_6 separation challenge by constructing suitable pore sizes and functional surfaces to take up more preferred C_2H_6 molecules.[9e,f,15] Although these works exhibit effectiveness for the separation of C_2H_4/C_2H_6, developing rational design strategies in the C_2H_6-selective adsorption field are still highly challenging. In this regard, our group developed a dynamic spacer installation (DSI) strategy to construct multi-functional MOFs by installing different spacers into the *proto*-MOF LIFM-28,[16] in which the pore space can be rationally partitioned, leading to small pore size, high pore volume, and functionalized pore surface, thus opening up a new avenue for realizing porous MOFs with multi-functionalization for C_2H_4/C_2H_6 separation.

Herein, we reported a series of multi-functional MOFs, LIFM-61/31/62/63 (LIFM stands for Lehn Institute of Functional Materials), through implementing dynamic spacer installation (DSI) strategy in the prototype MOF, LIFM-28, for removing C_2H_6 from C_2H_4/C_2H_6 mixtures. As shown in Scheme 1, a *proto*-LIFM-28 featured two types of replaceable coordination sites, that is, site A and site B, can be further assembled to generate more complicated structures. The *proto*-LIFM-28 presents two types of channels, i.e., smaller rhombic ones (pore size of approximately 7.2×10.9 and 5.1×7.3 Å^2) along the a- or b-axis (channel A and channel B), and larger orthogonal ones (11.1×11.1 and 7.0×7.0 Å^2) along the c-axis (channel C and channel D), both of which are not suitable for C_2H_4/C_2H_6 separation. Once the site A and site B in *proto*-LIFM-28 were installed with 1,4-dicarboxybenzene (H$_2$BDC), 2,6-naphthalenedicarboxylic acid (H$_2$NDC), biphenyl-4,4′-dicarboxylic acid (H$_2$BPDC), or 2′-methyl-[1, 1′ : 4′, 1′ terphenyl]-4, 4′′-dicarboxylic acid (H$_2$MTPDC) spacers, respectively, the pore sizes can be systematically reduced. Compared with the *proto*-LIFM-28, all the functionalized MOFs exhibit higher BET surface area and pore volume. Owing to the high pore volumes, they present enhanced C_2H_6/C_2H_4 adsorption performance, especially for LIFM-63, which can take up nearly three times as much C_2H_6 as the prototypical counterpart. Moreover, LIFM-63 features relatively smaller channel D and tetrahedral cages that were decorated with trifluoromethyl (-CF$_3$) and methyl (-CH$_3$) functional groups to facilitate the close contact between C_2H_6
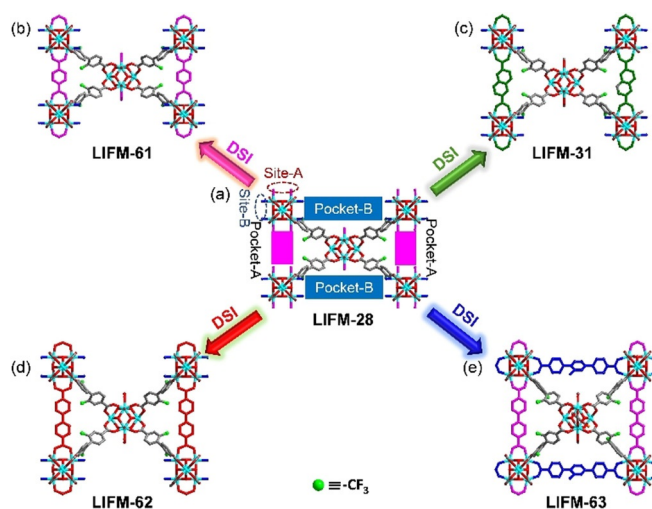

Scheme 1. Pore engineering of MOFs by dynamic spacer installation. a) The structure of LIFM-28 showing replaceable binding sites and pockets. b) The structure of LIFM-61. c) The structure of LIFM-31. d) The structure of LIFM-62. e) The structure of LIFM-63. H atoms are omitted for clarity.

molecules and the framework walls, leading to higher C_2H_6/C_2H_4 selectivity. Importantly, theoretical calculations and dynamic breakthrough experiments confirmed the result, in which the optimized pore space and pore surface of F, O atoms for C−H···F, C−H···O interactions and other van der Waals force (C−H···π) have a synergistic role in this C_2H_6/C_2H_4 separation challenge.

Results and Discussion

Synthesis and Structure Description

The *proto*-LIFM-28 was synthesized through the solvo-thermal reaction of H$_2$L^1 (H$_2$L^1 = 2,2′-bis(trifluoromethyl)-4,4′-biphenyldicarboxylate) and ZrCl$_4$ in *N,N*-dimethylformamide (DMF) solution according to our reported literature,[16a] featuring four pairs of replaceable -OH/H$_2$O terminates to form two types of binding sites, for example, site A along the *c*-axis and site B along the *a/b*-axis (Scheme 1 a). Two sites A form one pocket A adequate for the installation of linear dicarboxylate spacers with variable length ranging from BDC to BPDC spacers, whereas two sites B build one pocket B suitable for the immobilization of functionalized TPDC (triphenyl dicarboxylate) spacers. There are two types of channels, i.e., smaller rhombic ones (pore size of approximately 7.2×10.9 and 5.1×7.3 Å^2, taking into account of the van der Waals radii of the atoms) along the *a*- or *b*-axis (channel A and channel B), and larger orthogonal ones (11.1×11.1 and 7.0×7.0 Å^2) along the *c*-axis (channel C and channel D; Figure 1 a). After heating *proto*-LIFM-28 samples in *N,N*-dimethylformamide (DMF) solutions containing H$_2$BDC, H$_2$NDC, or H$_2$BPDC at 75 °C for 24 h, LIFM-61/31/62 were afforded, respectively. LIFM-63 was obtained by soaking *proto*-LIFM-28 into DMF solution containing both H$_2$BPDC and H$_2$MTPDC spacers at 85 °C for 40 h. LIFM-31
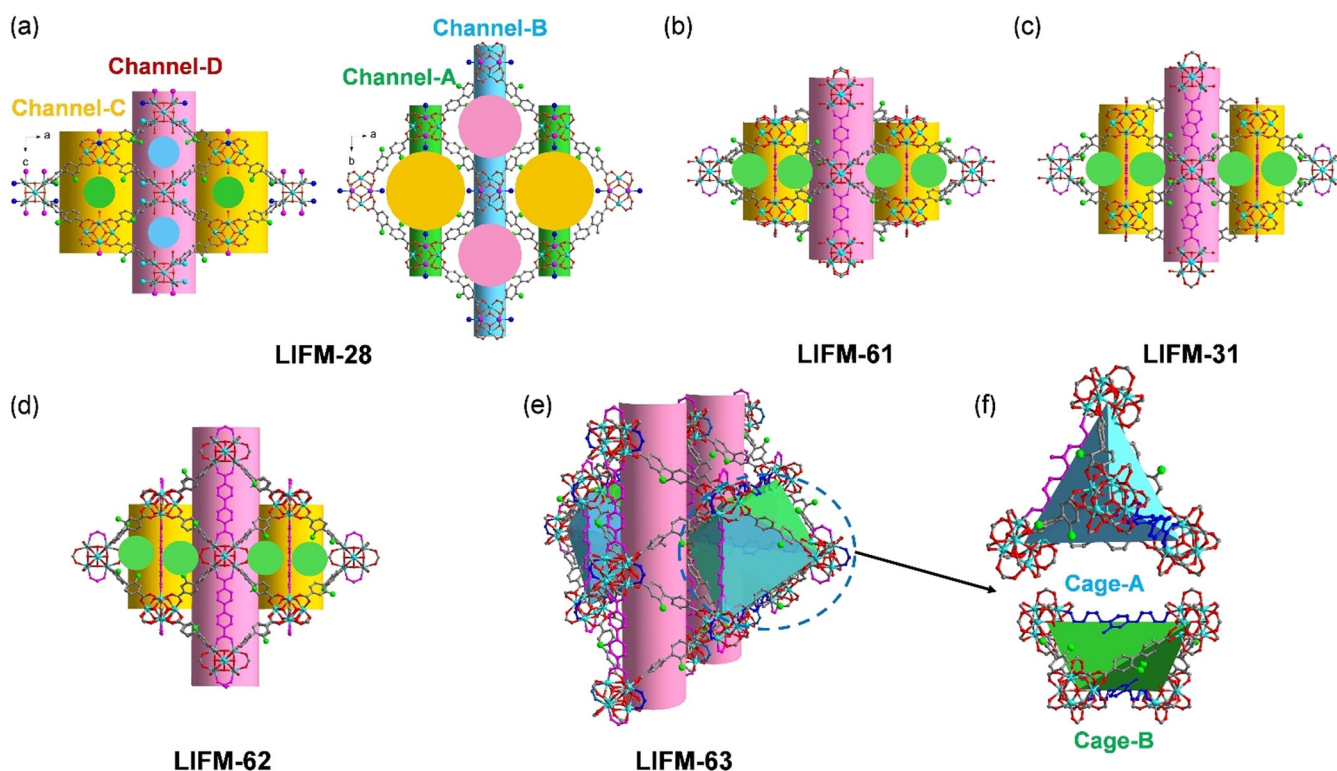
Figure 1. The schematic 3D structure of MOFs. a) LIFM-28. b) LIFM-61. c) LIFM-31. d) LIFM-62. e) LIFM-63. f) The tetrahedral cages in LIFM-63.

has been reported in our previous work.[16a] The structures of LIFM-61/62/63 were determined by single-crystal X-ray diffractions (SCXRD), in which BDC or BPDC spacers were precisely immobilized in pockets A (Scheme 1 and Figure 1), while MTPDC spacers were pinpointed in the pockets B (Scheme 1 and Figure 1). LIFM-61/62 are isostructural of LIFM-31 with the same *bct* topology, while LIFM-63 presents a *bcu-x* topology.[16b] The ratios of framework ligands and installed spacers in LIFM-61/31/62/63 have been confirmed by the ^1H NMR data of digested MOFs, identical with the theoretical values (see Figures S6–S9 and Table S2 in the Supporting Information). It is noteworthy that the channel B was entirely blocked, channel A was rationally compartmentalized into triangle pores with the aperture sizes of approximately 5.5×5.4 (LIFM-61), 5.5×5.6 (LIFM-31), and 7.0×5.7 (LIFM-62) $Å^2$, respectively. The sizes of channel D were changed to 7.3×7.3 (LIFM-61), 6.7×6.7 (LIFM-31), and 5.6×5.6 (LIFM-62) $Å^2$, respectively, whereas the sizes of channel C changed slightly with the aperture sizes of approximately 11.2×11.2 $Å^2$ decorated by -CF$_3$ groups, after installing BDC, NDC, and BPDC spacers into *proto*-LIFM-28 (Figure 1). Furthermore, when site A and B were installed with BPDC and MTPDC spacers, only the channel D was retained with the pore size of 5.6×5.6 $Å^2$ (Figure 1 e), while the other three channels A, B, and C were entirely blocked in the train of the formation of two tetrahedral cages, cage A and cage B (the aperture size is ca. 5.0 Å) functionalized by -CF$_3$ and -CH$_3$ groups that are useful for C$_2$H$_6$ capture (Figure 1 f). Notably, the DSI strategy has resulted in a significantly reduced pore size, increased pore volume as well as functionalized pore surface from proto-LIFM-28 to LIFM-61/31/62/63, presenting the potentials for enhanced confinement effects and multi-site

adsorption, especially for C$_2$H$_6$ with higher polarizability and more potential hydrogen bond receptors.

Phase Purity and Porosity

The phase purity of all the MOF samples has been confirmed by powder X-ray diffraction (PXRD) patterns (Figures S1–S5). The thermal stability of all the MOFs was examined by thermal gravimetric analyses (TGA) and variable-temperature-dependent PXRD (VT-PXRD) patterns, demonstrating enhanced stability after the DSI process (Figures S10–S13).[16a] N$_2$ adsorption experiments at 77 K were carried out to evaluate their porosity. As shown in Figure 2, all the MOFs show microporous type I sorption isotherms. The Brunauer-Emmett-Teller (BET) surface area and pore volume compared with *proto*-LIFM-28 (927 m^{2}g^{-1}, 0.41 cm^{3}g^{-1}) increase gradually after the installation of BDC, NDC, and BPDC spacers in pocket A, with the values of 1194 m^{2}g^{-1} and 0.49 cm^{3}g^{-1} for LIFM-61, 1711 m^{2}g^{-1} and 0.71 cm^{3}g^{-1} for LIFM-31, and 1977 m^{2}g^{-1} and 0.82 cm^{3}g^{-1} for LIFM-62, respectively, due to the expansion of spacer along with the main channels C and D via DSI (Table S3). For LIFM-63, its BET surface area (1486 m^{2}g^{-1}) and pore volume (0.62 cm^{3}g^{-1}) are also higher than *proto*-LIFM-28 but lower than LIFM-62 (Table S3). This phenomenon can be explained by the fact that the MTPDC spacer in pocket B further divides the channel C, which results in smaller pore space. Additionally, the pore size distribution (PSD) of all the MOFs was analyzed by DFT calculation, which exhibits a decreasing trend from *proto*-LIFM-28 (6.8 and 11.8 Å) to LIFM-63 (5.6 and 8.6 Å) (Figure S20). From the above results, it can be
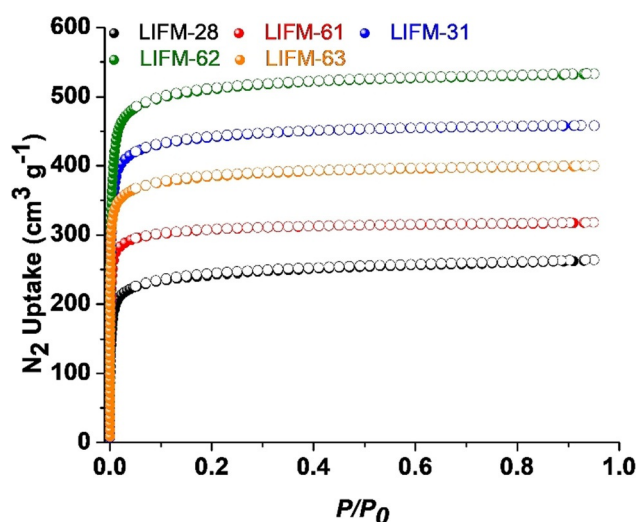
Figure 2. The N_2 adsorption of all the MOFs at 77 K.

concluded that the pore space and pore size can be finely tuned through DSI strategy, thereby displaying good potentials for specific selective gas adsorption.

C_2H_6 and C_2H_4 Adsorption

In order to evaluate the gas separation performance, we measured the C_2H_6 and C_2H_4 adsorption at 273 and 298 K. As depicted in Figure 3a and b, the installation of various spacers into *proto*-LIFM-28 significantly improves the C_2H_6 and C_2H_4 adsorption performance, especially for LIFM-63, representing nearly 3-fold increases compared to *proto*-LIFM-28. The difference in uptake of either C_2H_6 or C_2H_4 using *proto*-LIFM-28 are nearly similar, with values of 1.7 versus 1.1 mmol g^{-1} at 273 K and 1 bar (Figures 3c and S21–S24). Nonetheless, the C_2H_6 uptake amounts of LIFM-61/31/62/63 are 2.6, 4.0, 4.5, and 4.8 mmol g^{-1} at 273 K, respectively, which are much higher than C_2H_4 (2.1, 3.0, 3.3, and 3.7 mmol g^{-1}, respectively), especially for LIFM-63, implying the preferential binding affinity of the frameworks for C_2H_6 (Figures 3a–c and S21–S24). The C_2H_6 and C_2H_4 uptake capacities of LIFM-61/31/62/63 range from 1.7–3.0 and 1.4–2.1 mmol g^{-1} at 298 K and 1 bar, respectively, exhibiting similar trend to 273 K (Figures 3d and S21–S24). It is worth noting that small pore size usually correlates with small pore volume, resulting in low gas adsorption capacity; however, large pore size correlated with high pore volume exhibits poor selectivity of small gas molecules. Significantly, for LIFM-63, the C_2H_6 uptake capacity (3.0 mmol g^{-1}) under ambient conditions is higher than many reported MOFs like MAF-49 (1.70 mmol g^{-1}),[14a] ZIF-7 (2.24 mmol g^{-1}),[17] Cu(Qc)$_2$ (1.85 mmol g^{-1}),[9f] and Zn-atz-ipa (1.76 mmol g^{-1});[18] this observed amount is also comparable with the best MOFs, such as Fe$_2$O$_2$(dobdc) (3.3 mmol g^{-1}),[9e] ZIF-8 (or MAF-4) (3.5 mmol g^{-1}),[19] and PCN-245 (3.3 mmol g^{-1}),[20] which inherits from its collaborative effects of high pore volume and small pore size. Furthermore, the repetitive (5 cycles) C_2H_6 and C_2H_4 adsorp-
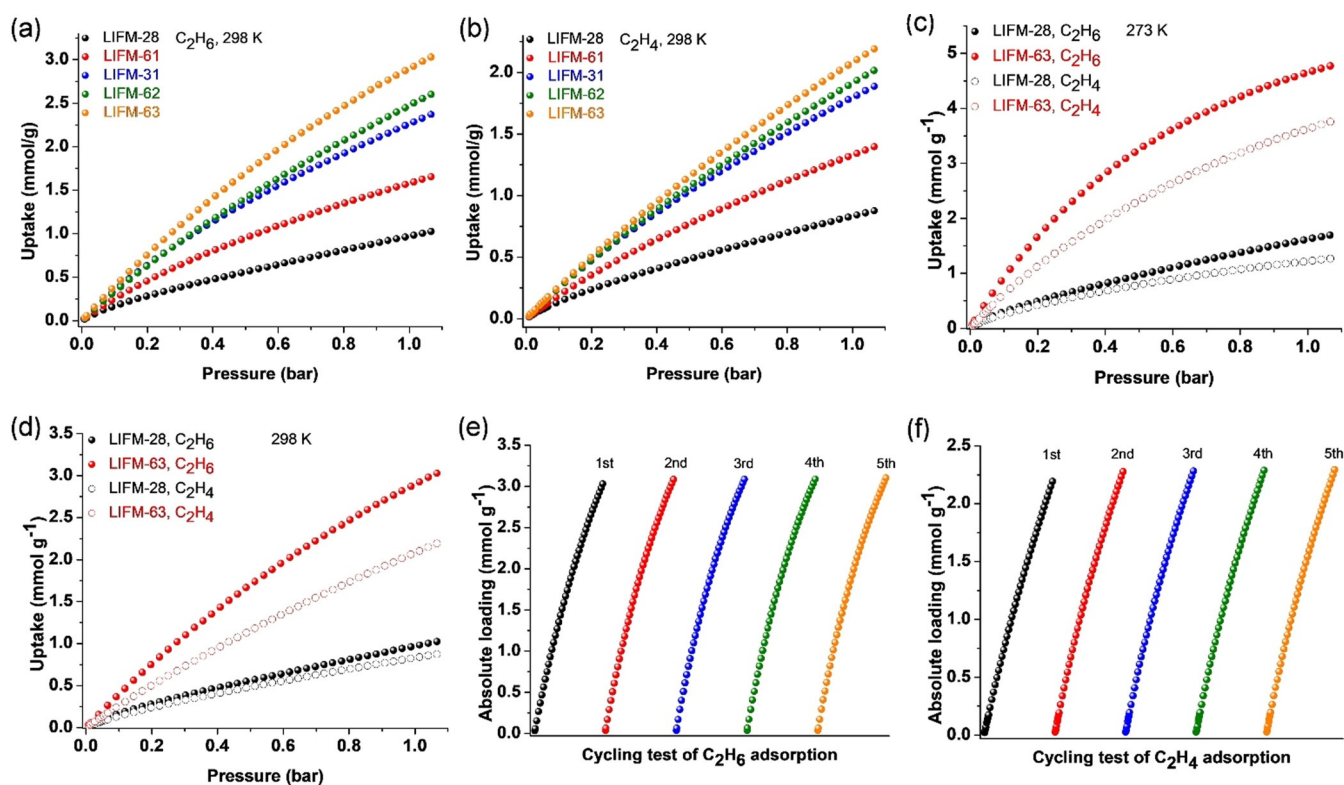

Figure 3. a) The C_2H_6 adsorption isotherms of all the MOFs at 298 K. b) The C_2H_4 adsorption isotherms of all the MOFs at 298 K. c) The C_2H_6 and C_2H_4 adsorption isotherms of LIFM-28 and LIFM-63 at 273 K. d) The C_2H_6 and C_2H_4 adsorption isotherms of LIFM-28 and LIFM-63 at 298 K. e) Repetitive C_2H_6 adsorption measurements of LIFM-63 at 298 K. f) Repetitive C_2H_4 adsorption measurements of LIFM-63 at 298 K.

tion experiments on LIFM-63 at 298 K were conducted carefully to confirm its excellent reusability, indicating a low regeneration energy requirement (Figures 3 e and f).

To investigate the binding mechanism, the coverage-depended adsorption enthalpy (Q_{st}) was calculated using the virial method based on the adsorption isotherms at different temperatures (Figures S27–S36). As depicted in Figures S37 and S38, the Q_{st} of C_2H_6 and C_2H_4 on LIFM-61/31/62/63 are similar as LIFM-28 at zero coverage and range from 24.1–26.9 and 24.9–27.5 kJ mol^{-1}, respectively, indicative of the similar gas-framework interactions. The Q_{st} of C_2H_6 and C_2H_4 on LIFM-63 are similar at zero coverage, but at high coverage the value for C_2H_6 is higher than that of C_2H_4, which indicates the enhanced intermolecular interactions among the adsorbates ascribing to the crystallographically observed small pore size and more H atoms of C_2H_6. Noteworthy, the Q_{st} of C_2H_6 on LIFM-63 is much lower than that of the benchmark adsorbents Fe$_2$O$_2$(dobdc) (66.8 kJ mol^{-1}),[9e] MAF-49 (60.0 kJ mol^{-1}),[14a] IRMOF-8 (52.5 kJ mol^{-1}),[14a] Zn-atz-ipa (45.8 kJ mol^{-1}),[18] further highlighting LIFM-63 as a promising candidate for C_2H_6/C_2H_4 separation with a low regeneration requirement.

To gain further insight into the unique C_2H_6 adsorption behavior in LIFM-63, theoretical calculations were implemented. The calculated binding energy for C_2H_6 is 33.4 kJ mol^{-1}, while it is 32.3 kJ mol^{-1} for C_2H_4, indicating a stronger binding affinity toward C_2H_6. The C_2H_6 guest is located in the electronegative pocket of cage B surrounded by one Zr$_6$ cluster, two L^1 ligands, and one MTPDC spacer, in which the strong C−H···F (2.70, 3.36, 3.74 and 3.82 Å), C−H···π interactions (2.86 and 3.56 Å), and weak van der Waals force (C−H···O distance ranges from 3.24 to 3.50 Å) occur between C_2H_6 and LIFM-63 (Figures 4a and S52). In comparison, C_2H_4 guest is located in the electronegative channel D surrounded by one Zr$_6$ cluster, two L^1 ligands, and one BPDC spacer, but exhibited weaker C−H···F (2.90 and 3.60 Å), C−H···π interactions (3.50 Å), and comparable van der Waals force (C−H···O distance ranges from 3.24 to 3.75 Å) (Figures 4b and S53). Therefore, the stronger binding energy for C_2H_6 can be attributed to the stronger C−H···F and C−H···π interactions. The theoretical calculations further demonstrated the effectiveness of the DSI strategy for constructing ideal adsorbents featuring high pore space and small pore size toward C_2H_6/C_2H_4 separation.

Prompted by the high adsorption capacity and preferred binding affinity for C_2H_6, we assessed the selectivity of C_2H_6/C_2H_4 gas mixtures on all the MOFs on the base of the ideal adsorbed solution theory (IAST) model[21] using the compo-

sition of 50:50 C_2H_6/C_2H_4 (Figures S39–S50). The sorption selectivity of C_2H_6 over C_2H_4 on LIFM-28 was estimated to be 1.33 and 1.24 at 273 and 298 K, 1 bar, respectively. In contrast, the values on LIFM-61/31/62/63 are higher than LIFM-28, especially for LIFM-63, with the values of 1.62 and 1.56 at 273 and 298 K, 1 bar, respectively (Figure 5 a and b). Notably, the MOFs have successfully achieved the combination of good adsorption selectivity and high uptake capacity through rationally regulating the pore space and pore environment with dynamic spacer installation approach.
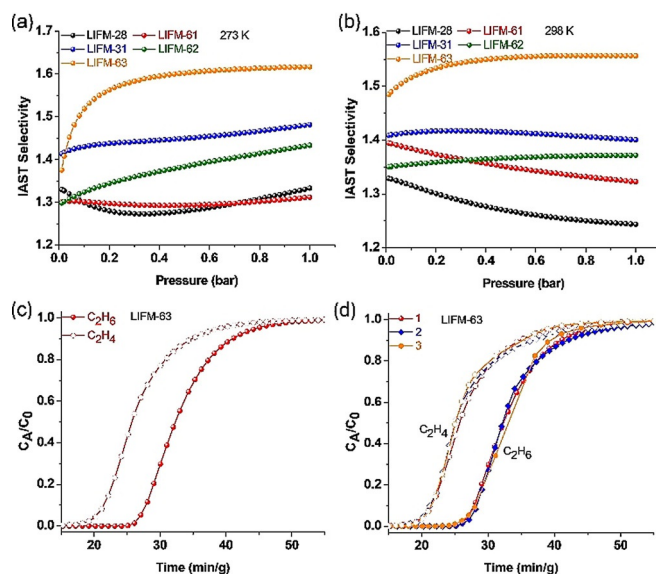
Figure 5. IAST adsorption selectivity of C_2H_6/C_2H_4 (v/v, 50:50) at 273 (a) and 298 K (b). c) The breakthrough curves of LIFM-63 for C_2H_6/C_2H_4 mixture at 298 K and 1 bar; and d) the cycling breakthrough curves of LIFM-63 for C_2H_6/C_2H_4 mixture at 298 K and 1 bar.

Afterward, to examine the practical dynamic adsorption selectivity performance, the transient fixed-bed breakthrough experiments of C_2H_6/C_2H_4 on LIFM-63 were carried out under ambient conditions, in which the C_2H_6/C_2H_4 (1/1, v/v) gas mixtures flow over a fixed-bed column with a rate of 4 mL min^{-1}. As shown in Figure 5 c, LIFM-63 presents an efficient separation of C_2H_6 over C_2H_4. The high-grade C_2H_4 (> 99.9 %) gas was first eluted without detectable C_2H_6, while C_2H_6 retained in the packed column until reaching its saturated uptake and then eluted. In addition, the multiple dynamic breakthrough experiments of C_2H_6/C_2H_4 on LIFM-63 were performed to evaluate its recyclability, showing the same C_2H_6 retention time as the first one (Figure 5 d). It should be noted that the regeneration of LIFM-63 is quickly through purging inert gas under ambient conditions, demonstrating its feasibility for actual industrial applications.

Conclusion

In summary, the dynamic spacer installation strategy has been successfully applied to construct multi-functional MOFs featuring high pore volume, small pore size as well as optimized pore surface for efficient C_2H_6/C_2H_4 separation.
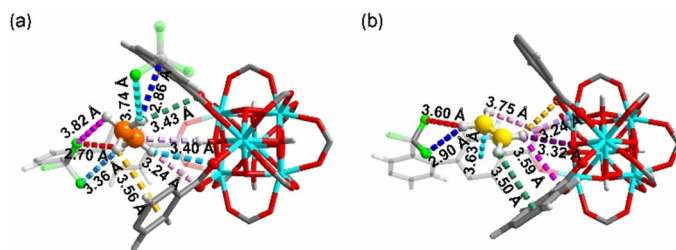
Figure 4. The preferential C_2H_6 (a) and C_2H_4 (b) binding sites of LIFM-63 observed by model studies.

Results showed that the installation of functional spacers into *proto*-LIFM-28 not only improved the pore volume but also reduced the pore size for enhanced C_2H_6/C_2H_4 adsorption and separation. Additionally, the framework stability has been enhanced by the DSI strategy. Owing to its high pore volume, small pore size, and optimized pore surface, LIFM-63 presents high C_2H_6 uptake capacity and good C_2H_6/C_2H_4 selectivity via stronger C−H···F and C−H···π interactions. Furthermore, the low adsorption enthalpy ensures that LIFM-63 can be regenerated easily through purging at ambient temperature over a short period time. Together with its robust framework stability, LIFM-63 can be successfully applied to the multi-recyclable C_2H_6/C_2H_4 adsorption separation process without performance deficiency. Significantly, this work represents another outstanding example of the DSI strategy for precisely regulating MOFs' pore environments for C_2H_6/C_2H_4 separation, thus facilitating the rational design of other novel MOFs materials for this challenging research.

Acknowledgements

Conflict of interest

The authors declare no conflict of interest.

[1] D. S. Sholl, R. P. Lively, *Nature* **2016**, *532*, 435–437.

[2] a) I. Amghizar, L. A. Vandewalle, K. M. Van Geem, G. B. Marin, *Engineering* **2017**, *3*, 171–178; b) T. Ren, M. Patel, K. Blok, *Energy* **2006**, *31*, 425–451.

[3] G. B. Kauffman, *Chem. Educ.* **2000**, *5*, 49–53.

[4] S. Chu, Y. Cui, N. Liu, *Nat. Mater.* **2017**, *16*, 16–22.

[5] a) J.-R. Li, R. J. Kuppler, H.-C. Zhou, *Chem. Soc. Rev.* **2009**, *38*, 1477–1504; b) K. Adil, Y. Belmabkhout, R. S. Pillai, A. Cadiau, P. M. Bhatt, A. H. Assen, G. Maurin, M. Eddaoudi, *Chem. Soc. Rev.* **2017**, *46*, 3402–3430; c) J. Kim, L.-C. Lin, R. L. Martin, J. A. Swisher, M. Haranczyk, B. Smit, *Langmuir* **2012**, *28*, 11914–11919; d) R. T. Yang, *Adsorbents: Fundamentals and Applications*; John Wiley & Sons, Inc.: NJ, **2003**.

[6] H. Golipour, B. Mokhtarani, M. Mafi, A. Moradi, H. R. Godini, *J. Chem. Eng. Data* **2020**, *65*, 3920–3932.

[7] G. Narin, V. F. D. Martins, M. Campo, A. M. Ribeiro, A. Ferreira, J. C. Santos, K. Schumann, A. E. Rodrigues, *Sep. Purif. Technol.* **2014**, *133*, 452–475.

[8] B. U. Choi, D. K. Choi, Y. W. Lee, B. K. Lee, S. H. Kim, *J. Chem. Eng. Data* **2003**, *48*, 603–607.

[9] a) Y. Chen, Z. Qiao, H. Wu, D. Lv, R. Shi, Q. Xia, J. Zhou, Z. Li, *Chem. Eng. Sci.* **2018**, *175*, 110–117; b) O. T. Qazvini, R. Babarao, Z.-L. Shi, Y.-B. Zhang, S. G. Telfer, *J. Am. Chem. Soc.* **2019**, *141*, 5014–5020; c) X. Wang, Z. Niu, A. M. Al-Enizi, A. Nafady, Y. Wu, B. Aguila, G. Verma, L. Wojtas, Y.-S. Chen, Z. Li, S. Ma, *J. Mater. Chem. A* **2019**, *7*, 13585–13590; d) H. Zeng, X.-J. Xie, M. Xie, Y.-L. Huang, D. Luo, T. Wang, Y. Zhao, W. Lu, D. Li, *J. Am. Chem. Soc.* **2019**, *141*, 20390–20396; e) L. B. Li, R. B. Lin, R. Krishna, H. Li, S. C. Xiang, H. Wu, J. P. Li, W. Zhou, B. L. Chen, *Science* **2018**, *362*, 443–446; f) R.-B. Lin, H. Wu, L. Li, X.-L. Tang, Z. Li, J. Gao, H. Cui, W. Zhou, B. Chen, *J. Am. Chem. Soc.* **2018**, *140*, 12940–12946; g) X. Zhang, L. Li, J.-X. Wang, H.-M. Wen, R. Krishna, H. Wu, W. Zhou, Z.-N. Chen, B. Li, G. Qian, B. Chen, *J. Am. Chem. Soc.* **2020**, *142*, 633–640; h) S.-K. Lee, Y. J. Lee, K. Cho, U.-H. Lee, J.-S. Chang, *Bull. Korean Chem. Soc.* **2021**, https://doi.org/10.1002/bkcs.12179.

[10] a) Y. He, R. Krishna, B. Chen, *Energy Environ. Sci.* **2012**, *5*, 9107–9120; b) E. D. Bloch, W. L. Queen, R. Krishna, J. M. Zadrozny, C. M. Brown, J. R. Long, *Science* **2012**, *335*, 1606–1610; c) J. E. Bachman, M. T. Kapelewski, D. A. Reed, M. I. Gonzalez, J. R. Long, *J. Am. Chem. Soc.* **2017**, *139*, 15363–15370; d) Z. Bao, S. Alnemrat, L. Yu, I. Vasiliev, Q. Ren, X. Lu, S. Deng, *Langmuir* **2011**, *27*, 13554–13562.

[11] a) L. Zhang, L. Li, E. Hu, L. Yang, K. Shao, L. Yao, K. Jiang, Y. Cui, Y. Yang, B. Li, B. Chen, G. Qian, *Adv. Sci.* **2019**, *7*, 1901918; b) S. Aguado, G. Bergeret, C. Daniel, D. Farrusseng, *J. Am. Chem. Soc.* **2012**, *134*, 14635–14637; c) B. Li, Y. Zhang, R. Krishna, K. Yao, Y. Han, Z. Wu, D. Ma, Z. Shi, T. Pham, B. Space, J. Liu, P. K. Thallapally, J. Liu, M. Chrzanowski, S. Ma, *J. Am. Chem. Soc.* **2014**, *136*, 8654–8660.

[12] A. Jayaraman, R. T. Yang, C. L. Munson, D. Chinn, *Ind. Eng. Chem. Res.* **2001**, *40*, 4370–4376.

[13] A. Mersmann, B. Fill, R. Hartmann, S. Maurer, *Chem. Eng. Technol.* **2000**, *23*, 937–944.

[14] a) P. Q. Liao, W. X. Zhang, J. P. Zhang, X. M. Chen, *Nat. Commun.* **2015**, *6*, 8697; b) Z. Xu, X. Xiong, J. Xiong, R. Krishna, L. Li, Y. Fan, F. Luo, B. Chen, *Nat. Commun.* **2020**, *11*, 3163; c) H. Yang, Y. Wang, R. Krishna, X. Jia, Y. Wang, A. N. Hong, C. Dang, H. E. Castillo, X. Bu, P. Feng, *J. Am. Chem. Soc.* **2020**, *142*, 2222–2227.

[15] A. A. Lysova, D. G. Samsonenko, K. A. Kovalenko, A. S. Nizovtsev, D. N. Dybtsev, V. P. Fedin, *Angew. Chem. Int. Ed.* **2020**, *59*, 20561–20567; *Angew. Chem.* **2020**, *132*, 20742–20748.

[16] a) C.-X. Chen, Z. Wei, J.-J. Jiang, Y.-Z. Fan, S.-P. Zheng, C.-C. Cao, Y.-H. Li, D. Fenske, C.-Y. Su, *Angew. Chem. Int. Ed.* **2016**, *55*, 9932–9936; *Angew. Chem.* **2016**, *128*, 10086–10090; b) C. X. Chen, Z. W. Wei, J. J. Jiang, S. P. Zheng, H. P. Wang, Q. F. Qu, C. C. Cao, D. Fenske, C. Y. Su, *J. Am. Chem. Soc.* **2017**, *139*, 6034–6037.

[17] C. Gücüyener, J. van den Bergh, J. Gascon, F. Kapteijn, *J. Am. Chem. Soc.* **2010**, *132*, 17704–17706.

[18] K.-J. Chen, D. G. Madden, S. Mukherjee, T. Pham, K. A. Forrest, A. Kumar, B. Space, J. Kong, Q.-Y. Zhang, M. J. Zaworotko, *Science* **2019**, *366*, 241–246.

[19] Y. Wu, H. Y. Chen, D. F. Liu, Y. Qian, H. X. Xi, *Chem. Eng. Sci.* **2015**, *124*, 144–153.

[20] D. F. Lv, R. F. Shi, Y. W. Chen, Y. Wu, H. X. Wu, H. X. Xi, Q. B. Xia, Z. Li, *ACS Appl. Mater. Interfaces* **2018**, *10*, 8366–8373.

[21] A. L. Myers, J. M. Prausnitz, *AIChE J.* **1965**, *11*, 121–127.